Influence of Chain Topology on Polymer Dynamics and Crystallization. Investigation of Linear and Cyclic Poly(ε-caprolactone)s by ^{1}H Solid-State NMR Methods

Kerstin Schäler,[*,†] Elena Ostas,[‡] Klaus Schröter,[§] Thomas Thurn-Albrecht,[§] Wolfgang H. Binder,[‡] and Kay Saalwächter[*,†]

[†]Institut für Physik-NMR, Martin-Luther-Universität Halle-Wittenberg, Betty Heimann-Strasse 7, 06120 Halle/Saale, Germany

[‡]Chair of Macromolecular Chemistry, Institute of Chemistry, Division of Technical and Macromolecular Chemistry, Martin-Luther-Universität Halle-Wittenberg, von-Danckelmann-Platz 4, 06120 Halle/Saale, Germany

[§]Institut für Physik-Polymer Physics, Martin-Luther-Universität Halle-Wittenberg, von-Danckelmann-Platz 3, 06120 Halle/Saale, Germany

ⓢ *Supporting Information*

ABSTRACT: We report on the investigation of cyclic and comparable linear poly(ε-caprolactone)s (PεCL) with molecular weight between 50 and 80 kg/mol with regard to chain mobility in the melt and crystallinity using low-field solid-state ^{1}H NMR. Our results from NMR Hahn echo and more advanced multiquantum measurements demonstrate a higher segmental mobility of cyclics in the melt as compared to their linear counterparts. Rheological experiments indicate that the cyclics are less viscous than the linear analogues by about a factor of 2, confirming the NMR results. FID component analysis shows higher crystallinities of the cyclic samples by some percent under the condition of isothermal crystallization at 48 °C, suggesting that due to their enhanced overall mobility in the melt, the cyclics reach a more perfect morphology leading to higher crystallinity. We compare this finding with results from DSC measurements obtained under identical conditions and critically evaluate the applicability of polymer crystallinity determination from nonisothermal crystallization investigations by DSC. We further highlight the use of nucleating agents to investigate the particular effect of crystal growth on (nonisothermal) crystallization, separated from the influence of nucleation. These experiments indicate a faster crystal growth for cyclic samples.
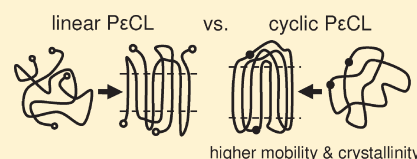
INTRODUCTION

For creating optimized polymer structures, profound knowledge of polymer crystallization is necessary. However, up to now this process has still not been understood completely on a molecular scale. Besides the classical model of crystallization kinetics by Hoffman and Lauritzen based on the assumption of a successive, thermally activated attachment of single chains to the crystal growth front,[1] also collective local ordering processes of several polymer chains at once[2,3] as well as spinodal-like processes are under discussion.[4] Although polymer crystals can exhibit numerous morphologies with hierarchies of molecular organization, still it remains unclear, what determines them to evolve. Furthermore, the influence of chain topology and molecular weight as well as the role of the entanglements prior to and during crystallization has not been entirely clarified yet and is the subject of ongoing discussion.[5−13] Thus, the mechanisms involved in the crystallization of entangled polymers have recently attracted renewed attention.[2,14−18] In this context, we investigate the influence of chain topology on polymer crystallization, addressing this issue by comparing crystallinity and chain mobility of cyclic polymer chains (free of loose chain ends) and linear chains with the same number of monomer units.

Cyclic polymers are supposed to adopt "lattice-animal"-like conformations which incorporate double-folded loops and may be percolated by loops of neighboring chains.[19,20] They are attractive systems for exploring basic phenomenological models, e.g., to investigate the influence of highly mobile chain ends on chain dynamics and the physical properties of the material,[20−24] reptation processes which seem to be unavailable for rings,[20] percolation,[25] or chain folding[26,27] phenomena. Comprehensive investigations on cyclic PDMS have been done by Semlyen and co-workers, starting from pioneering work on ring−chain equilibria in the 1960s, continuing with larger-scale synthesis and characterization of cyclic PDMS in the late 1970s, and applying almost every available characterization method to these samples in the ensuing decades.[24,28−35] Other cyclic polymer systems such as cyclic PS and PB have since then been synthesized and characterized.[20,22,23] Apart from ring-closure reactions of linear chains, new and more defined synthetic strategies (relying on cyclic initiators via ROMP, ROP, "click"-reactions or ring-expansion
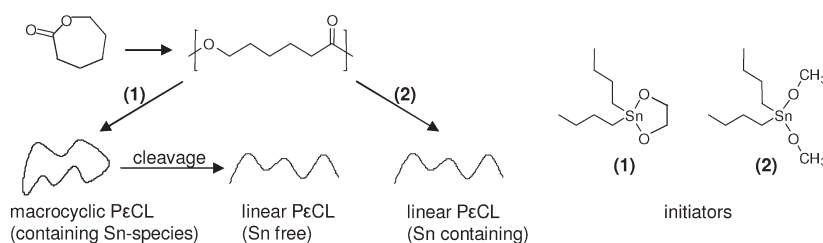
Figure 1. Synthetic approach for the preparation of cyclic and linear PεCL.

polymerization[36−38]) allow extensive investigations of ring polymers also in the semicrystalline state.

Studies on cyclic polymers to explore macromolecular self-organization processes such as the formation of the semicrystalline state are particularly rare. Up to now, there are a few phenomenological reports on DSC characteristics of cyclic systems of higher molecular weight,[33,39,40] but detailed studies appear to be limited to monodisperse cyclic alkanes (poly(ethylene)) and poly(ethylene oxide)s of low and medium molecular weights.[26,27] Such systems exhibit crystallinities close to 100% and almost perfect crystal structures with closely packed and integer-folded chains. Thus, they cannot be representative models for the investigation of crystallization mechanisms of highly entangled polymers.

Here we study poly(ε-caprolactone) (PεCL), a biodegradable, semicrystalline polyester of medium crystallinity and a convenient melting temperature of around 60 °C at high molecular weight (MW > M_e). The crystallization behavior of the linear form has been studied in detail, for instance by Strobl[41−45] for a given molecular weight. Linear PεCL crystallizes in lamellae in a planar zigzag conformation within an orthorhombic unit cell. The ester groups are slightly twisted from the plane of the planar zigzags.[46] Solid-state NMR investigations of Kaji and Horii[47] showed that the crystalline CH_2 sequences perform fast conformational fluctuations while the carbonyl groups remain virtually rigid. Their observations of monoexponential T_1 relaxation times suggest the absence of large-scale chain motion in the crystallites, classifying PεCL as a crystal-fixed polymer[48] and therefore an interesting system for general investigations on polymer crystallization.

PεCLs of cyclic[49] and other topologies (such as dendritic,[50] tadpole-shaped,[39] and star-shaped[51]) have been synthesized in the past decade with high precision. Diverse results on the influence of topology on the thermal behavior of various PεCL-polymers have been reported, but more detailed investigations on the crystallization behavior of cyclics beyond the simple observation of nonisothermal crystallization temperatures in DSC experiments are rare. Results on topological effects seem to have in common that the crystallization behavior changes according to the chain topology, mostly expressed by a significant reduction of the crystallization tendency with decreasing large-scale chain mobility and increasing steric hindrance of the individual polymer chains.

Here, we survey the crystallization of linear and comparable cyclic PεCL chains at molecular weights between 50 and 80 kg/mol by means of low-field solid-state ^1H NMR methods. In addition, we report on some earlier measurements for an extended molecular-weight range (15−110 kg/mol), for which the samples were less ideal as far as their storage and temperature treatment was concerned. As NMR experiments are sensitive to the segment mobility of polymer chains via anisotropic residual dipolar couplings, they provide the opportunity to investigate semicrystalline polymers in terms of chain mobility and entanglement dynamics in the melt state,[52] and also structural properties such as crystallinity[53] and domain sizes (via spin diffusion[54,55]) can be derived. The residual local order and mobility of polymer chain segments is accessible via simple Hahn echo measurements or more advanced multiquantum (MQ) NMR experiments, whereas the crystallinity information can be deduced from the intensity of the free induction decay (FID) curve.

In this paper, we will first describe sample preparation and characterization and then present results on chain mobility in the molten samples from solid-state NMR relaxation and MQ experiments compared to data from rheological measurements. Moreover, we will give a comparison of the crystallization behavior of linear and cyclic counterparts, as studied by solid-state NMR and DSC after isothermal crystallization. There, we also address the influence of chain topology on crystallization in nonisothermal DSC studies, separating crystal growth information from effects of nucleation by using externally nucleated PεCL samples.

■ POLYMER SYNTHESIS AND EXPERIMENTAL TECHNIQUES

Polymerization. A 20 mL polymerization flask was carefully heated (400 °C) and purged with argon. After cooling the flask was silanized. Donor−acceptor interactions between hydroxyl groups on the glass surface and tin atoms of the initiator (O→Sn) induce a competition reaction to the interaction between monomer and initiator which can prevent the insertion of monomer into the metal−oxygen bond and consequently may cause a broad polydispersity and a decrease in the yield of the polymerization. In order to remove all hydroxyl groups from the glass surface, a 10% solution of dichlorodimethylsilane in absolute dichloromethane was given into the flask and stirred for 1 h. Then the dichlorodimethylsilane solution was removed rapidly, the flask was purged with argon and closed by means of a cap with septum.

Before polymerization, ε-caprolactone (purchased from Aldrich Co.) was stirred over calcium hydride overnight and then distilled off into a flask and closed with a septum immediately. The pure ε-caprolactone was transfused via a syringe into the closed polymerization flask. In the case of initiator **1** (Figure 1) it was dissolved in 4 mL of absolute toluene at 100 °C and transfused via syringe into the polymerization flask. In the case of initiator **2** (Figure 1), it was used without any solvent. Different amounts of ε-caprolactone and initiator were needed depending on the intended molecular weight of the polymer, e.g., for a cyclic sample with $M_{n,GPC}$ = 45.0 kg/mol we used 2 g (4 × 10^{-5} mol) of ε-caprolactone and 0.012 g (4 × 10^{-5} mol) of initiator **1**. The polymerization flask was immersed into a thermo-regulated oil bath for 24 h. When the reaction time

was over, the product was dissolved in dry CH_2Cl_2 and precipitated into cold diethyl ether (5 °C), filtered off and dried in vacuum overnight.

GPC. Gel permeation chromatography (GPC) measurements were done at a Viscotek GPCmax VE 2001 with a Styragel linear column GMH$_{HR}$. Tetrahydrofuran (THF) was used as a carrier-solvent at 1 mL/min at room temperature. The sample concentration was approximately 3 mg/mL. Polystyrene standards ($M_p = 1050-115000$ g/mol) were used for conventional external calibration, using a Waters RI 3580 refractive index detector.

Rheology. Rheological measurements were done using a Rheometrics Dynamic Analyzer RDAII from TA Instruments with a parallel plate geometry. The diameter of the sample was 25 mm and the thickness around 1.7 mm. In this case compliance effects of the instrument are negligible. Shear loss modulus (G'') and storage modulus (G') were determined as a function of frequency from 1 to 100 rad/s. Typically, the strain in the sample was 2%, being well within the linear deformation range. The strain was chosen to keep the measured torque values in a range of about 100 to 0.2 g·cm, corresponding to the measurement range of the transducer of the instrument. At low frequencies, the decreasing modulus values and hence also torque values limit the useful measurement range for the rheometer.

For sample preparation, the polymer powder was pressed under vacuum in a cylindrical mold with the desired diameter and thickness. After 8 h at 90 °C, the sample was slowly cooled down to room temperature overnight under vacuum. The cylindrical polymer sample was placed between the two plates of the rheometer and after heating to 90 °C and slight compression it stuck to the surface of the parallel plates. Subsequently, the temperature was lowered to the measurement temperature of 60 or 80 °C and equilibrated. During these temperature changes the thermal expansion of the tools of the instrument was compensated by a corresponding change of the gap setting. Because of the air and humidity sensitivity of cyclic PεCL all the measurements were conducted under a nitrogen gas flow.

NMR Spectroscopy. The nuclear magnetic resonance (NMR) time-domain measurements were conducted using 0.5-T Bruker minispec mq20 low-resolution NMR spectrometers (19.9 MHz proton Larmor frequency, 90° and 180° pulses of ∼2.2 to 3.0 μs and ∼4.6 to 5.6 μs length, respectively) equipped with a commercial wide temperature range static probe.

For the NMR measurements about 0.3 g of PεCL sample each were molten to cover the bottom of 8 mm (diameter) sample tubes and flame-sealed under vacuum conditions, in order to avoid degradation of the samples due to atmospheric O_2 and water. The sample temperature was regulated by means of a BVT3000 heater working with air as a heating gas. The sample tubes were centered in the middle of the coil region by custom-made Teflon spacers. The average sample temperature was measured by an external thermometer; small temperature gradients in the order of 0.5 K over the sample length cannot be excluded. All time-domain NMR signals were recorded applying on-resonance conditions and in full-absorption mode receiver setting. To make sure that the longitudinal relaxation was complete between the scans in the semicrystalline state as well as in the melt, the recycle delay was set to 1.2 s.

Crystallinity Measurements. In order to remove melt memory effects, all the samples were molten and kept at 90 °C for about 30 min and then rapidly placed into a thermostat for isothermal crystallization at (48 ± 1) °C for 4−5 days (depending on the order of the measurements). For crystallinity

measurements the samples were directly transferred from the thermostat into the preheated spectrometer (again (48 ± 1) °C) and measured one after the other. In this way, the crystallization time was extended for the last samples investigated. At this time the primary crystallization was finished and only secondary crystallization was still continuing. However the increase in crystallinity during this waiting period (∼1.2% from first to last measurement) is smaller than the measurement uncertainty. The crystallinities were determined by analyzing MSE-refocused FIDs.[53,55]

Measurement of Chain Mobility in the Melt. In order to remove all melt memory effects, each sample was molten, kept at 90 °C for approximately 30 min, and then directly transferred into the preheated spectrometer (80 °C). Information about the degree of local order induced by nonisotropic chain motions was derived from proton homonuclear residual dipolar couplings investigated by Hahn echo and multiple-quantum NMR measurements.

DSC. Differential scanning calorimetry (DSC) was carried out with a Perkin-Elmer DSC7 and a Perkin-Elmer Pyris Diamond instrument calibrated with indium and mercury or indium and cyclopentane, respectively. Samples of 5 to 10 mg were encapsulated in pressure-tight 30 or 50 μL aluminum pans. Nitrogen was used as purge gas. The data were evaluated by means of Pyris Thermal Analysis version 3.81 or Pyris Thermal Analysis version 5.00.02, including a baseline subtraction for all nonisothermal measured DSC curves.

For evaluation of the crystallinity after isothermal crystallization each sample was pretreated nonisothermally by keeping it in the melt at 90 °C for 10 min, cooling to 0 °C at −10 K/min, holding at 0 °C for 10 min and reheating to 90 °C. After 10 min in the melt the sample was rapidly cooled (at −200 K/min or highest possible cooling rate) to the crystallization temperature of 48 °C and isothermally crystallized for a crystallization time t_c. From the subsequent heating scan to 90 °C at 10 K/min heat flow and enthalpy of fusion were determined. To allow a check for consistency the pretreatment steps were repeated.

To investigate the nonisothermal crystallization the melting and crystallization temperatures (evaluated at the peak onsets) were deduced from heat flow curves during heating to 100 °C (after cooling the melt from 100 °C to 0 °C and holding it at 0 °C for 10 min) and a second cooling run to 0 °C after holding at 100 °C for 10 min. All cooling and heating steps were conducted at 10 K/min.

The glass transition temperatures of the amorphous regions of the semicrystalline samples were measured upon heating to 85 °C at 20 K/min after having cooled the sample from the melt to −100 °C at 20 K/min and annealing for >10 min. The glass transition was visible and the glass transition temperatures T_g were determined as the midpoints of the glass transition steps. The T_g values do not differ by more than 1 to 2 °C. Within the scatter no significant trend concerning a differentiation between linear and cyclic samples can be seen. Hence, also at higher temperatures (i.e., in the melt) we do not expect significant deviations of the segmental dynamics between linear and cyclic chains caused by free volume differences.

■ EXPERIMENTAL RESULTS AND DISCUSSION

Sample Preparation and Characterization. Cyclic PεCL samples were prepared by insertion polymerization according to procedures reported by Kricheldorf et al.[56] For the ring-opening

Table 1. Representative Sample Properties As Obtained by GPC, Rheology, Solid-State NMR, and DSC

	sample 1		sample 2		sample 3		sample 4	
	linear	cyclic	linear	cyclic	linear	cyclic	linear	cyclic
M_n [kg/mol][a]	50.6	45.0	63.4	57.5	69.2	64.0	77.0	69.0
M_w/M_n[a]	1.6	1.6	1.6	1.6	1.8	1.8	2.1	2.1
$\eta_{\omega \to 0}$ [Pa·s] (60 °C)			4867	2748	6987	3917		
$\eta_{\omega \to 0}$ [Pa·s] (80 °C)			2371	1288	3355	1879		
T_2 [ms] (80 °C)	4.3	6.1	4.3	7.2	4.4	9.7	3.9	8.1
$f_{c,NMR}$[b]	0.48	0.54	0.48	0.55	0.48	0.55	0.48	0.52
$f_{c,DSC}$[b]	0.48	0.53					0.48	0.54
$T_{m,DSC}$ [°C] (Onset)[c]	53.7	53.3					54.1	54.2
$T_{c,DSC}$ [°C] (Onset)[c]	35.0	36.4					36.1	36.8

[a] From GPC; despite the equal number of monomers of corresponding linear and cyclic samples a smaller value of M_n is obtained for cyclic samples due to smaller hydrodynamic radii. [b] After isothermal crystallization. [c] For nonisothermal crystallization of non-nucleated sample.
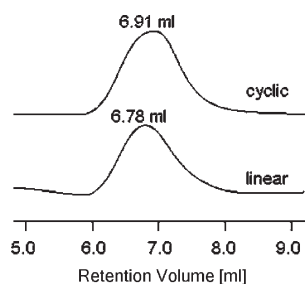
Figure 2. GPC traces with indicated retention volume for one pair of linear (M_n = 63.4 kg/mol, M_w/M_n = 1.6) and corresponding cyclic (M_n = 57.4 kg/mol, M_w/M_n = 1.6) sample.

polymerization of ε-caprolactone we used an Sn-based cyclic initiator (2,2-dibutyl-1,2-dioxa-2-stannane) (**1** in Figure 1) which does not allow for the concatenation of rings. The corresponding linear polymers were obtained directly from the respective cyclic PεCLs by cleavage of the Sn—O bond with 1,2-ethanedithiol to yield bis-hydroxytelechelic PεCL.[57] They exhibit the same number of monomers as their cyclic counterparts and are free of tin.

Molecular weights ranging from M_n ∼15 kg/mol to ∼110 kg/mol for the linear samples were determined by GPC measurements. The polydispersities varied between 1.6 and 2.1 (for examples see Table 1). During formation of linear chains from cyclics the initiator (MW = 233 g/mol) is eliminated. As this small molecular weight difference is within the GPC uncertainty, equal molecular weights for linear and corresponding cyclic samples were to be expected from GPC. Yet, we find higher retention volumes for the cyclic PεCLs compared to the values of the corresponding linear samples (Figure 2). The molecular weights for the cyclic PεCLs therefore appear to be lower than for their linear analogues. This is because in comparison to the linear counterpart with the same number of monomers the expected hydrodynamic radius for a cyclic is lower[37] as linking both ends of a linear polymer chain reduces the overall dimensions of the chain. Our finding confirms the successful synthesis of rings and allows to distinguish between the cyclic and corresponding linear chains.
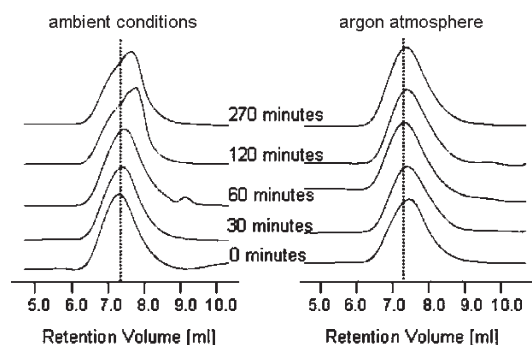
Figure 3. GPC traces of a linear tin-containing PεCL (M_n = 28.6 kg/mol, M_w/M_n = 1.7) at 95 °C under ambient conditions (moisture and oxygen) and under argon. The bottom traces (t = 0 min) show the sample state before cleavage. The measurement times during the cleavage experiment are indicated.

The absence of tin signals (originating from the initiator **1**) in MALDI—TOF spectra of our cyclic samples (see Supporting Information) prompted us to check the degradation of the polymers under our experimental conditions. For this purpose, we used linear, tin-containing samples prepared by means of a second initiator (dibutyl-tin-dimethoxide) (**2** in Figure 1). By cleaving the Sn—O bond, these polymers separate into two parts of about half the molecular weight, providing a significant change in GPC retention volume, that can be more clearly detected than the small difference between a cyclic sample and its linear counterpart (see also Figure 2). The sample was placed in a sealed glass tube and heated to 95 °C either under ambient conditions (moisture and oxygen) or under an atmosphere of argon, and the molecular weights were monitored by GPC in regular time intervals. As can be seen in Figure 3, heating under ambient conditions afforded a significant overall reduction in molecular weight and the appearance of a second peak at higher retention volume (lower molecular weight), whereas under an atmosphere of argon no significant change in molecular weight and therefore no Sn—O-bond cleavage was visible. Accordingly, further measurements had to be conducted under exclusion of air and moisture and the samples were stored under vacuum. Similar degradation results are also known from Hoskins and Grayson[49] for PεCL rings synthesized by click chemistry.

Chain Mobility of Linear and Cyclic Samples. *Melt Rheology Investigations.* Rheological experiments in the melt provide information about the molecular dynamics and the spectrum of relaxation times of a polymer system, which depends critically on chain architecture. It was recently pointed out that compared to linear chains a melt of rings exhibits additional relaxation modes, but no rubber plateau.[20] Such changes in the time dependent shear modulus $G(t)$ also lead to a different viscosity η.

Figure 4a shows the storage- and loss modulus G' and G'' of a pair of linear and corresponding cyclic PεCL sample at 60 °C demonstrating that the moduli of the cyclic polymer both are significantly lower than the moduli of the corresponding linear one. The storage modulus G' deviates from the asymptotic power law behavior for both samples. This may be of experimental origin or due to a distribution of terminal relaxation times (polydispersity effect). The fact that G' for the ring system is lower than for the linear system is consistent with the expectation of a stronger relaxation due to additional modes. The loss modulus G'' approaches terminal flow behavior, with $G'' = \eta \cdot \omega$ being a direct measure for the viscosity.
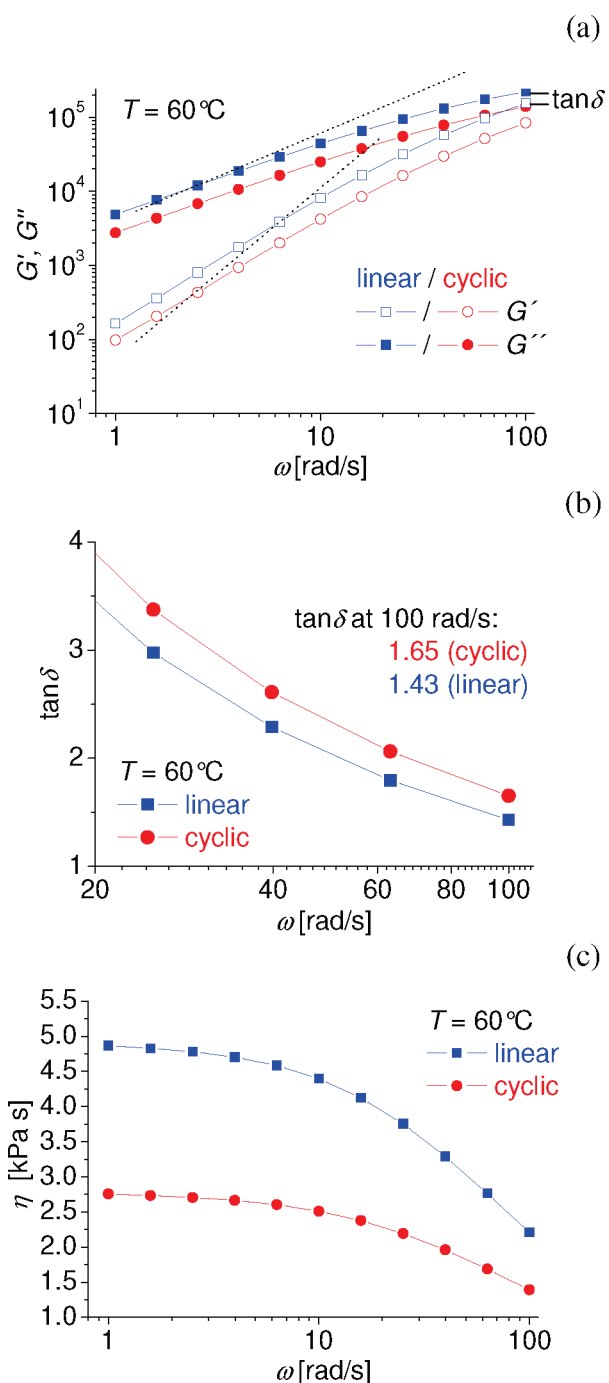
Figure 4. Melt rheology measurements for one pair of linear and cyclic PεCL samples with $M_{n,lin} = 63.4$ kg/mol measured at 60 °C . (a) Storage modulus (G') and loss modulus (G'') as a fuction of shear frequency. The broken lines correspond to functions proportional to ω^2 and ω^1 according to the asymptotic limits for G' and G''. (b) Loss tangent tan δ and (c) melt viscosity as calculated from part a.

As can be seen from Figure 4a at high frequencies ω the crossover point of G' and G'' of the linear sample is not quite reached and measurements at lower temperatures which could have been used to extend the measurement range were not possible due to crystallization setting in below 60 °C . However, the value of tan $\delta = G''/G'$ at the highest frequency measured (100 rad/s) is smaller for the linear than for the cyclic system (see

Figure 4b). These data seem to suggest that also for the cyclic PεCL a crossover point exists but compared to the linear sample this point is shifted to higher frequencies, indicating that due to higher flexibility and/or mobility the cyclic chains are able to follow the fast shear motion in the high frequency range more easily than their linear analogues.

The viscosities η of the two samples are explicitly demonstrated in Figure 4c (for numerical values see Table 1), which shows $\eta = G''/\omega$ as a function of shear frequency. Here we observe that the viscosity of the ring system is lower than for the linear system by nearly a factor of 2. The higher fluidity of the melt of rings is consistent with the faster relaxation of rings as compared to the linear chains.[20] Similar results have been described in the past, e.g. by McKenna et al.[58] and Roovers[22] who showed for polybutadiene (M_w between 50 and 200 kg/mol) that the melt viscosity of the cyclics can be a factor of 10 lower than for the linear counterparts, yet it is known that even minute linear-chain contaminants can obscure such a large contrast. We checked all our findings from melt rheology measurements for another pair of samples and for both sample pairs at a higher temperature of 80 °C (see Table 1) yielding comparable results.

In conclusion the rheological properties of the systems under study show clear differences in line with expected trends demonstrating independently that indeed rings have been synthesized. Nevertheless there are contaminations of the ring systems with opened linear chains the extent of which we cannot definitely evaluate but, after comparing our results with viscosity data in ref 20, expect to be on the percent level.

NMR Hahn Echo Measurements. Apart from rheology measurements also ^{1}H NMR T_2 relaxation time studies provide information about the chain mobility in polymer melts, using the orientation-dependent ^{1}H homonuclear residual dipolar coupling strength as an observable. Highly mobile polymer chains show a slow transverse relaxation with a long corresponding relaxation time T_2. This behavior is caused by motional averaging of proton dipolar couplings due to the fast, nearly isotropic movements of the molecules. Polymer chain entanglements or packing constraints posed by neighboring chains form topological restrictions which hinder the faster segmental motions (Rouse modes). Thus, they induce an anisotropy of chain motion (on the NMR time scale) and local order to a certain degree.[52] Consequently residual dipolar couplings persist due to an incomplete averaging and the outcome is a faster transverse relaxation and a lower T_2 value. Hence the analysis of the transverse relaxation behavior at temperatures far above T_g can provide information about the density of topological constraints (e.g., entanglements) and/or the time scale of large scale chain motion.[52]

To investigate the transverse relaxation behavior of linear and cyclic PεCLs in the melt, we measured Hahn echo decay curves[59] at 80 °C . For one pair of linear and corresponding cyclic sample ($M_{n,lin} = 63.4$ kg/mol from GPC) the results are shown in Figure 5. Approximate T_2 times are summarized in Table 1. The initial nonexponential shape of the decay curves suggests that effects due to residual dipolar couplings dominate the behavior. This is not uncommon for polymer melts with high molecular weight.

For our linear samples we find a faster relaxation behavior than for the cyclics. This difference hints at a stronger motional anisotropy in the linear PεCLs as compared to the cyclic ones, resulting from more or stronger restrictions to fast chain
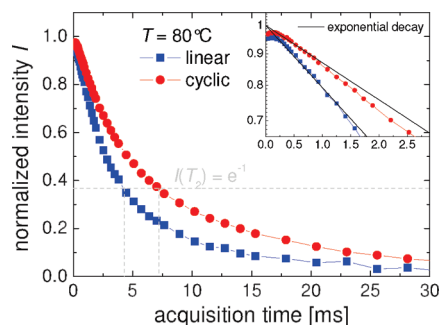
Figure 5. Transverse relaxation curves obtained from low-field ^{1}H NMR Hahn echo measurements in the melt at 80 °C for a pair of linear and corresponding cyclic PεCL with $M_{n,lin}$ = 63.4 kg/mol. The inset points out the nonexponential initial shape of the decay curves.
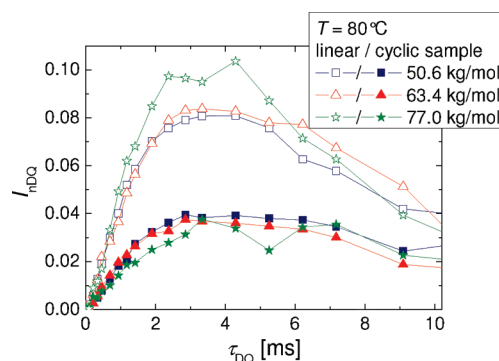

Figure 6. Normalized double-quantum intensities for linear (open symbols) and corresponding cyclic samples (full symbols) with different molecular weights (from GPC).

mobility. This could be either due to enhanced entanglement or packing effects (as from the polymer theoretical point of view cyclics adopt "lattice-animal"-like conformations rather than forming entanglements[19,20]) and/or a longer time needed for isotropic large scale motions (reptation). This finding is in agreement with the results from melt rheology, where a higher viscosity was determined for linear PεCL.

NMR Multiple-Quantum Measurements. As Hahn echoes have the drawback that information about residual dipolar couplings can hardly be separated from spin relaxation induced by fast thermal motion and that the relaxation curve is influenced by many unknown factors,[52,60] we alternatively performed ^{1}H NMR multiple-quantum (MQ) experiments to study the chain mobility of linear and respective cyclic PεCL samples.

MQ NMR is a selective tool for the determination of weak residual dipolar couplings in polymeric systems, i.e., polymer melts. Here, we used a pulse sequence of variable duration τ_{DQ} (a compensated version of an early MQ experiment of Baum and Pines) to excite even multiquantum coherences and to reconvert them into observable magnetization.[52] This approach yields two qualitatively different sets of data from one experiment: (i) an intensity build-up I_{DQ} which is among other things related to dipolar coupled segments (denoted double-quantum filtered signal) and (ii) a reference decay curve I_{ref}, which (besides half of the quantum orders of the dipolar coupled segments) also consists of contributions from noncoupled components. This portion contains e.g. dangling chains, loops and chain ends, showing rapid, isotropic mobility. Thus, the NMR signal relaxation is slow. The sum of both data sets is used to normalize the double-quantum filtered intensity I_{DQ} by point-by-point division, thus removing relaxation effects. Hence a normalized build-up curve I_{nDQ} is obtained, whose initial increase is related to the residual dipolar coupling strength D_{res} and residual order in the sample and is independent of the time scale of fast segmental fluctuations. In principle the shape of this curve can also provide information about the distribution of residual dipolar couplings and semilocal dynamic heterogeneities. Details on the theoretical background and applicability of the method are given by Vaca Chávez and Saalwächter.[52,61−63]

MQ experiments and data analysis were performed following procedures that are specified elsewhere.[52,61] The double-quantum intensities I_{DQ} obtained for our samples are very small compared to network samples due to large scale dynamics which are not existent in a network. As can be seen from Figure 6 build-up curves I_{nDQ} are received for the samples investigated,

confirming again that residual dipolar couplings and local order are present in the samples. Because of the polydispersity of the samples a tail subtraction as described in refs 52 and 61 was not possible. The normalized intensities presented here are therefore smaller than shown in these references.

Comparing the results for linear and corresponding cyclic PεCL samples, we find normalized build-up curves I_{nDQ} with a smaller initial slope and intensity for the cyclics. In the region of the steepest increase ($\tau_{DQ} \sim 1$ ms) the build-up intensity of the linear samples is about 2.5 times as large as for the cyclics. This observation again points to a stronger motional anisotropy and higher residual local order in the linear PεCLs due to more or stronger hindrances to fast chain mobility, which are posed by entanglements and/or packing constraints caused by neighboring chains. The findings coincide with the conclusions from our rheology and Hahn echo measurements in the melt, where cyclic samples showed a higher mobility as well.

As we expected, we find a slight increase in build-up intensity with rising molecular weight for the linear chains, as longer chains tend to form more entanglements, thus inducing a higher degree of motional anisotropy. This trend cannot be seen from the Hahn echo relaxation curves where it is probably masked by dynamic effects (arising from intermediate motions of the dipolar coupling tensor[63]). We attribute the overall weak molecular-weight effects to the narrow MW range and the after all considerable polydispersities that are always larger than 1.6, which means that the MW distributions of all samples overlap significantly. Future in-depth studies on the details ring vs chain dynamics should thus be carried out with more narrowly dispersed samples. We do not find a molecular weight trend for the cyclic samples neither from the multiquantum measurements nor from the Hahn echo curves, probably as a result of contaminations with linear chains. The impurity contents are small but unequal for all cyclic samples examined. Although their effect on the NMR experiment should not be dominant (see below) it may become noticeable at this point.

For short τ_{DQ} (region of initial rise) the normalized intensity I_{nDQ} is directly proportional to the orientation autocorrelation function of the second Legendre polynomial $C(t) = \langle P_2(\cos \theta(t)) \cdot P_2(\cos \theta(0)) \rangle$, with θ being the angle of the segmental orientation relative to the external magnetic field.[62]

$$\frac{I_{nDQ}}{\tau_{DQ}{}^2} \sim C(\tau_{DQ}) \sim D_{res}{}^2 \qquad (1)$$
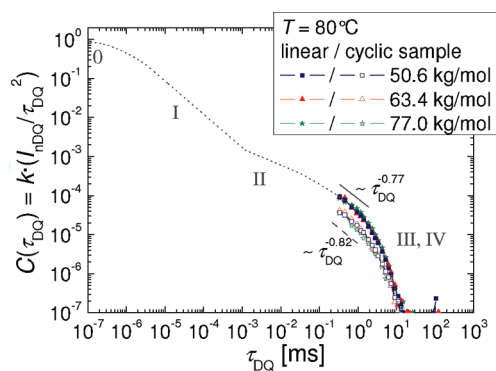
Figure 7. Correlation function $C(\tau_{DQ})$ (in arbitrary units) as calculated from I_{nDQ}/τ_{DQ}^2 for linear (full symbols) and corresponding cyclic (open symbols) PεCL samples at 80 °C. The dotted line indicates a constructed autocorrelation function for $Z = 11$ based on experimental data for PB, PI, and PDMS,[61] with corresponding Doi—Edwards tube-model regimes indicated as Roman numerals.

The autocorrelation function describes long-lived orientation correlations caused by semilocal anisotropy or, to put it simply, the loss of orientational memory of the chain segments. As it is proportional to the time dependent shear modulus $G(t)$ our NMR data can be compared directly to rheology data from literature. Conducting shear measurements in a melt of polystyrene rings Kapnistos et al.[20] showed that in the presence of small amounts of linear chains a percolation network of linear and cyclic chains is formed throughout the sample having rather "linear" shear properties compared to the pure melt of rings. By contrast NMR MQ experiments have the advantage that the signal is not as sensitive to an admixture of linear chains to the melt of rings. As the NMR signal only comprises contributions of each single chain it does not "see" the macroscopic percolation.

For the linear and corresponding cyclic PεCL samples $I_{nDQ}/\tau_{DQ}^2 \sim C(\tau_{DQ})$ is shown as a function of τ_{DQ} in Figure 7. Despite the (rather small) differences in molecular weight we perceive no significant deviation of the initial curve decays of our linear samples owing to a distribution of residual dipolar coupling strengths, probably as a consequence of polydispersity. The same can be concluded directly from the initial rise of the build-up curves in Figure 6. It is rather linear instead of having an inverted Gaussian shape, as expected for a single residual dipolar coupling strength.

To obtain information about the specific Doi—Edward tube-model regimes[61,63] explored by our measurements, we deduce a relaxation power law exponent from the initial decay of the measured data curves shown in Figure 7. As it is known from literature for a melt of linear chains, in the free Rouse regime I the decay of the correlation function adopts an apparent exponent of -0.85, which increases when passing over to entangled dynamics at the entanglement time τ_e.[61,64] In the constrained-Rouse Regime II where chain motions become anisotropic because of constraints posed by neighboring chains the scaling exponent ε depends on molecular weight, taking values between -0.4 and -0.45 in the case of our PεCL samples with an average number of entanglements per chain Z between 6 and 16 (with $Z = M_{n,lin}/M_e$ and M_e between 3000 and 5000 g/mol[65,66]). In regime III, which is dominated by chain reptation, the correlation function decay steepens before crossing over to regime IV (free, isotropic chain diffusion). The value of the corresponding scaling exponent

changes from -0.5 near the Rouse time τ_R to -1.5 being reached at the disentanglement time τ_d.[61]

The entanglement time τ_e can approximately be evaluated by using the relation $\tau_e \simeq 4\tau_\alpha N_e^2$ found for PB by Vaca Chávez and Saalwächter,[61] with τ_α being the α-relaxation time at the measurement temperature, known from dielectric measurements,[67] and N_e denoting the number of Kuhn segments between two entanglements. For PεCL, using the Kuhn segment length of 7 Å[68] and M_e for a rough calculation, we obtain a value of N_e between 30 and 50, which seems to be too large as compared to the value $N_{e,PB} \simeq 15$ found for PB,[61] considering that M_e of both polymers is similar. Yet, it is in the same range. For our samples we thus estimate τ_e to be in the order of 10^{-6} s. As this is significantly shorter than the time range of our measurements (see Figure 7), we conclude that with our MQ experiments we probe chain dynamics far beyond regime I. Furthermore, with a scaling exponent of about -0.77 (having a high uncertainty of ± 0.15 because of bad statistics and small signal intensities), the decay exponent found for our linear samples is in the range expected for regime III, confirming the presence of reptation-like dynamics in these samples at 80 °C. Note that the potential of reducing the measurement temperature to obtain information on e.g. constrained-Rouse dynamics (regime II) is limited by the fact that crystallization already occurs below 60 °C.

From rheology measurements by Kapnistos et al.[20] on PS (Z between 8 and 11 with M_e around 17.5 kg/mol) we know, that in contrast to linear chain stress relaxation via reptation cyclic chains exhibit additional relaxation modes. The resulting stress relaxation proceeds faster and follows a power law. This difference is expressed in the stress relaxation modulus of the cyclic PS being lower than for the corresponding linear samples above the entanglement relaxation time τ_e. The correlation functions of our cyclic PεCL samples are placed beneath the ones of the linear samples (Figure 7), thus reflecting Kapnistos' results. The power law exponent extracted from the correlation function of the cyclic samples (-0.82 ± 0.20) is also lower than yet still similar to the one of the linear samples. In accordance to this result, the time-dependent shear moduli of the samples have very similar log—log slopes for linear and cyclic samples as well (see Figure 4a).

Crystallinity of Linear and Cyclic Counterparts. *^{1}H Solid-State NMR Magic Sandwich Echo (MSE) Measurements after Isothermal Crystallization.* As solid-state NMR is sensitive to segmental mobility, it can be used to study phase composition in polymers based on heterogeneities in molecular mobility. The observable quantity is again the dipolar coupling strength which depends directly on the mobility of the polymer chain segments. Charlesby and Bridges[69] were the first who measured NMR time domain signals (free induction decay, FID) in order to study the crystallization behavior of polymers. Such NMR experiments represent a simple and fast alternative to DSC or scattering studies.

The FID obtained from semicrystalline polymers is a superposition of contributions from protons in

(i) rigid crystallites,
(ii) liquid-like mobile amorphous regions, and
(iii) so-called "rigid-amorphous" regions with intermediate mobility.[42]

The strong dipolar interactions between proton spins in the crystallites cause a dephasing and a fast initial drop in the signal which can be used to determine the sample crystallinity.[70]

During the receiver dead time (approximately 12 μs for our low-field equipment) a significant fraction of the quickly decaying rigid-part signal vanishes so that the crystallinity information cannot be deduced directly from the FID. To overcome this problem we used a pulsed version of the mixed magic sandwich echo sequence (MSE) before signal detection, which serves to refocus the dipolar dephased signals and provides a reasonably long final delay to cover the dead time. The pulse sequence is described in detail elsewhere.[53,55] Note that a phase inversion of the second "sandwich" pulse ensures the complete refocusing of chemical shifts. Signal from liquid-like sample fractions thus does not decay appreciably during the echo.

After isothermal crystallization of the linear and corresponding cyclic PεCL samples for some days the dipolar-refocused FIDs were recorded at the crystallization temperature of 48 °C . The refocusing of the FID by the MSE sequence proved to be almost quantitative and does not have much effect on the signal shape at the measurement temperature. Because of this observation we can indirectly exclude the presence of intermediate mobility (10−100 kHz) in the crystallites, which is for instance present in poly(ethylene) or poly(ethylene oxide), where chains diffuse in/through the crystallites. Note that at low temperatures (<0 °C in the case of PεCL) FID component analysis is not suitable to determine crystallinity as the mobility of the amorphous fraction decreases, rendering the corresponding signal unseparable from the rest.

We here summarize details of the signal analysis, as it turned out that the experimental procedure had to be adapted to the special case of PεCL. The most important specific point concerns the functional form assumed to describe the shapes of the crystalline, rigid-amorphous and amorphous signal contributions to the refocused FID. As in many inorganic crystals and glasses a small beat or oscillation is observed in the FID of PεCL being the result of strong dipolar interactions of neighboring proton spins in the crystallites. Structural information about these protons can in principle be obtained by conducting a moment analysis of the FID using a Taylor series expansion with the moments of line shape. This approach yields a a function similar to the Abragam function,[71,72] which provides a good analytical description of the oscillation in the FID in the case of PεCL. The amorphous part signal is influenced by the inhomogeneity of the magnetic field and can most conveniently be described by a stretched exponential.[53] It turned out that for a complete reproduction of the FID a third fit component for an interfacial signal part is necessary. Thus, for the phase-resolved analysis of the refocused FID curves, we fitted the initial 200 μs of the signal decay for all samples with a weighted superposition of

(i) an Abragam function $\exp(-a^2t^2/2)(\sin bt)/(bt)$ representing the crystalline signal contribution,

(ii) a stretched exponential $\exp(-t/(T_{2a}^*))^{\nu_a}$ representing the amorphous part signal, and

(iii) another stretched exponential $\exp(-t/(T_{2ra}^*))^{\nu_{ra}}$ representing the rigid-amorphous part signal.

The fixed shape parameters T_{2a}^* and ν_a for the amorphous part signal were independently obtained by fits to filtered data, based on an amorphous-phase specific "MAPE" (magic and polarization echo) filter (of length 0.87 ms);[73] see Figure 8. The shape parameters of the rigid-amorphous and the crystalline signal varied freely. For more details on the fitting strategy, see ref 55. The crystallinity f_c and the amorphous and rigid-amorphous fractions f_a and f_{ra} are given by the weighting factors of the three
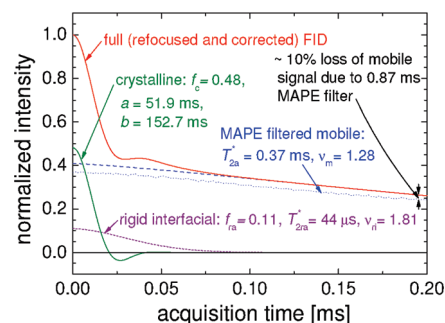

Figure 8. Refocused FID curve of a linear PεCL sample with M_n = 63.4 kg/mol at 48 °C and decomposition into the signals from the different phases. The presented data are already corrected for signal loss due to the MSE and renormalized.
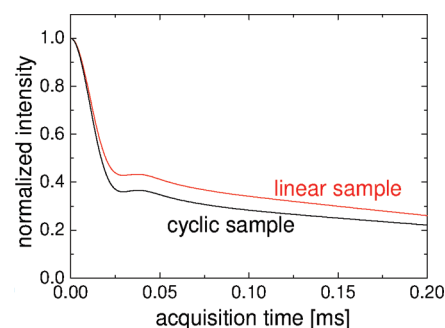

Figure 9. Corrected and normalized refocused FID curves of a cyclic (lower black curve) and linear PεCL sample (upper red curve) with M_n = 63.4 kg/mol at 48 °C.

signal contributions, respectively. As these values depend on the choice of the filter time for the experiment-based determination of the mobile signal shape, they are apparent quantities, which may be subject to a systematic error of a few percent that is the same for all samples investigated. A phase-specific correction of intensities was necessary because of a small signal loss due to the refocusing echo. It was done by quantitative comparison of the fit curve for the refocused FID with a nonrefocused FID. The correction factors for f_c, f_a, and f_{ra} are in the range of 1.10 to 1.14, 1.01 to 1.03, and 1.05 to 1.13 respectively for the present samples. After this correction we renormalized the fractions such that $f_c + f_{ra} + f_a = 1$.

Fitting results for a corrected data set are presented in Figure 8. The apparent crystallinity f_c of 48% obtained here is close to the 42% crystallinity given by Kaji and Horii for a ^{13}C-based measurement of a PεCL of ∼80 kg/mol isothermally crystallized at 50 °C and measured at 41 °C.[47] The crystallinity turned out to increase reversibly at temperatures below the isothermal crystallization temperature, in our case by about 7% for a temperature change of 18 °C . Uncertainties of the obtained fractions may arise from the measurement statistics (<0.5%), secondary crystallization, the fitting and correction procedure and small temperature deviations during the measurements. We estimate the overall uncertainty to be smaller than or around 5% for f_c and f_a and smaller than 10% for f_{ra}. (The given errors are scaled to the respective fractions.)

Figure 9 displays typical FID curves for a pair of linear and corresponding cyclic polymer. Already from the raw data we can conclude that more protons reside in the amorphous regions for
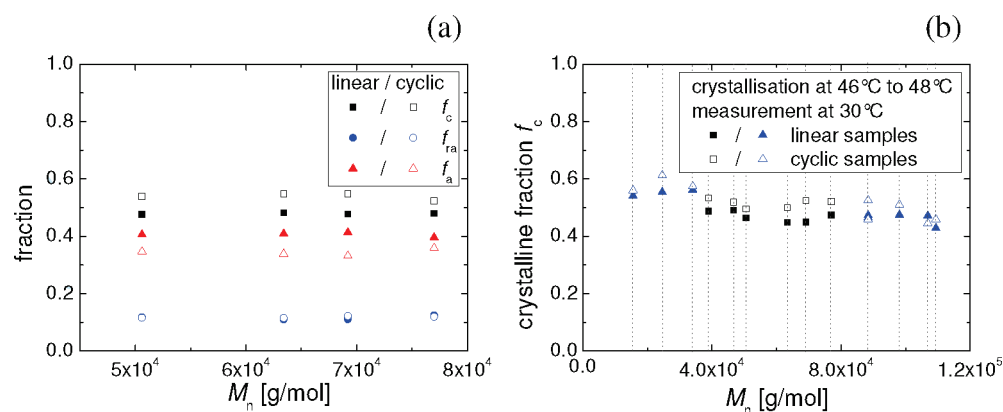
Figure 10. (a)Crystalline (f_c), amorphous (f_a), and rigid-amorphous (f_{ra}) fractions of cyclic (open symbols) and linear (full symbols) PεCL, obtained after isothermal crystallization at 48 °C by low-field NMR at 48 °C and (b) crystallinity f_c of cyclic (open symbols) and linear (full symbols) PεCL for a wider range of molecular weights measured at 30 °C after isothermal crystallization at 46 to 48 °C and temporary storage at room temperature. Results originating from an older sample batch are depicted as triangles.

linear polymers compared to cyclics. The essential results of the component decomposition of all samples are shown in Figure 10a. Here, the crystalline fractions of the cyclic polymers are higher by several percent than in the linear counterparts ($\sim$54% as compared to $\sim$48%). The amorphous fractions show the corresponding inverted trend, and consequently, the rigid-amorphous fractions do not reveal any correlation with the polymer type.

The same trend continues also for a wider range of molecular weights as presented in Figure 10b. These data originate from a previous series of experiments, and partly also from an older sample batch, the treatment of which was less well documented. At that time, we only had sparse information about the dependency of the crystallinity on measurement and crystallization temperature and about the time development of the secondary crystallization process. Thus, we crystallized the samples at 46–48 °C for some days and performed crystallinity measurements at 30 °C during the subsequent days after a temporary storage of the samples at room temperature over a varying period of time. Despite this less reproducible temperature pretreatment, the crystallinity results are in full agreement with the tendency described above. We are thus confident that the present findings are valid for this much expanded molecular-weight range.

From the fit parameters a and b in the Abragam function, we calculated the second moment of line shape $M_2 = a^2 + b^2/3$. The values of $\sim$10.4 $\times$ 10^9 s^{-2} obtained for all samples do not show differences for linear and cyclic PεCL.

DSC Measurements after Isothermal Crystallization. To confirm the NMR results on crystallinity we performed DSC measurements for two of the sample pairs ($M_{n,lin}$ = 77.0 kg/mol and 50.6 kg/mol). We chose a DSC temperature program that is comparable to the procedure used to determine the sample crystallinities by NMR measurements (see Polymer Synthesis and Experimental Techniques) comprising a long isothermal step at 48 °C and a subsequent heating scan. To check if the measured data are consistent we conducted one set of cooling and heating scans before and after the steps belonging to the isothermal crystallization. The corresponding heat flow curves match well, indicating that a quantitative analysis in terms of crystallinity is reasonable.

From the heat flow during the heating scan subsequent to the isothermal crystallization step we calculated heat capacity (C_p)

curves taking into account the sample mass and correcting the baseline. Furthermore, we determined the melt of fusion ΔH_m from the peak area in the C_p curves. From this value we calculated the crystallinity f_c by normalization with the theoretical value for the melt of fusion of 100% crystalline PεCL ΔH_m^0:

$$f_{c,\mathrm{DSC}} = \frac{\Delta H_m}{\Delta H_m^0}$$

The values for ΔH_m^0 given in the literature scatter between 135 J/g and 148 J/g.[39,47,74−76] The latter was calculated as the difference between the temperature dependent enthalpy functions of amorphous and crystalline PεCL at 48 °C.[76,77] (A value of ΔH_m^0 = 157 J/g stated by Wurm et al.[78] is given for the equilibrium melting temperature T_m^0 = 69 °C.)

To select a reasonable duration for the isothermal DSC step we tracked the development of crystallinity during isothermal crystallization at 48 °C for one of the linear samples online in the NMR spectrometer using the method described above (Figure 11a). By means of this information we chose the duration of the isothermal step to be 200 min to make sure that the primary crystallization was finished. A second DSC measurement using an isothermal step of 20 min duration helped us to estimate the temperature deviation between NMR and DSC measurement. As it turned out, the time axis of the NMR curve had to be scaled by a factor of 1.3 to match the DSC and NMR crystallinity results (Figure 11a). According to isothermal crystallization experiments we performed on linear PεCL for varying temperatures by NMR, this "shift" corresponds to a temperature difference of about 1 °C between the measurement temperatures of the NMR spectrometer and the DSC equipment. This is in the order of the experimental uncertainty.

The NMR crystallinity measurements have been performed after 4 to 5 days of isothermal crystallization. However, for the reason for practicability the crystallization time for the DSC experiments has been restricted to 200 min. To obtain comparable crystallinity results from both types of measurement we had to account for the prolonged crystallization time in the case of the NMR experiment by correcting the DSC crystallinities by means of a factor of 1.12 considering the expected 12% of additional increase in crystallinity during secondary crystallization (Figure 11a).
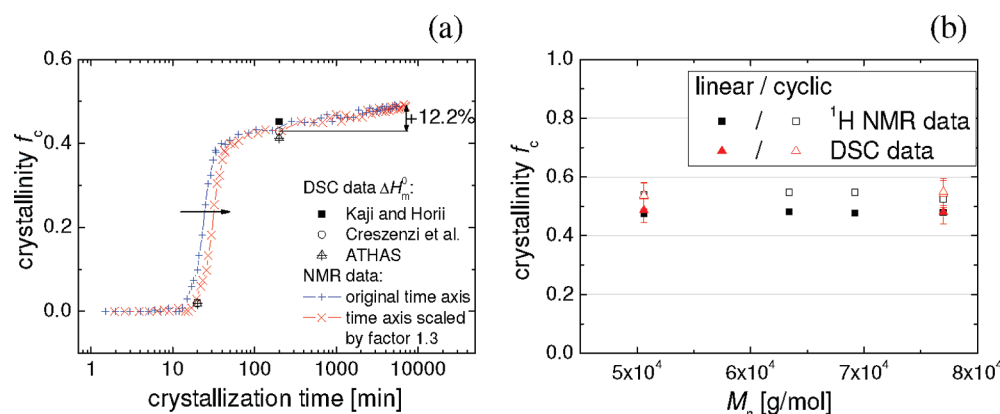
Figure 11. (a) Development of crystallinity f_c during isothermal crystallization at 48 °C tracked by ^{1}H NMR MSE measurements in comparison with crystallinity data from DSC measurements after isothermal crystallization calculated for different values ΔH_m^0 (from literature) for a linear PεCL sample (M_n = 77 kg/mol). The NMR curve needs to be time-scaled by a factor of 1.3 to match the DSC results indicating a temperature deviation between both measurements of ~1 °C. To consider the prolonged crystallization time in the case of the NMR measurement a further increase of crystallinity has to be taken into account. (b) Crystallinity determined from NMR and DSC measurements as a function of molecular weight for pairs of linear and corresponding cyclic PεCL samples.
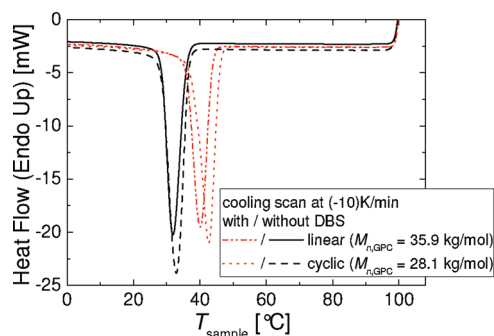

Figure 12. Heat flow curves for a pair of linear ($M_{n,GPC}$ = 35.9 kg/mol; solid and dash-dotted line) and corresponding cyclic ($M_{n,GPC}$ = 28.1 kg/mol; dashed and dotted line) sample with and without nucleating agent from a cooling scan at a cooling rate of −10 K/min. The heat flow curves for the non-nucleated sample pair are shown in black (solid and dashed) whereas data from the samples blended with the nucleating agent (DBS) are marked in red (dash-dotted and dotted).

As can be seen in Figure 11a, the heat of fusion for an infinite PεCL crystal ΔH_m^0 = 142.4 J/kg given by Creszenzi et al.[74] (average of the values listed there) fits our data best. The crystallinities determined by using this value are shown in Figure 11b in comparison with the corresponding NMR results. They match the NMR data nicely, confirming the suitability of the NMR experiment and our analysis procedure. The good agreement shows that possible contributions of a rigid-amorphous fraction to the DSC melting peak integral do not pose a problem here. The uncertainty of the DSC crystallinities settles at 5 to 6% and mainly results from the scattering of the ΔH_m^0 values given in the literature. It is similar to the uncertainty of our NMR crystallinities.

Use of Nucleating Agents: Nonisothermal Crystallization Investigated by DSC. As nonisothermal DSC measurements are a standard method for the determination of polymer crystallinity we also investigated heat flow and C_p curves for the nonisothermal crystallization and melting during a cooling and the subsequent heating scan for one pair of linear and cyclic samples with $M_{n,lin}$ = 35.9 kg/mol.

Analyzing the onsets of the crystallization and melting peaks we find a slightly higher crystallization temperature T_c of the cyclic sample in comparison to the corresponding linear one (36.5 °C as compared to 35.8 °C, see Figure 12) but no significant difference between the melting temperatures T_m of linear and cyclic samples. The fraction of crystalline material formed under nonisothermal conditions and determined from the peak area of the heating scan C_p curves in terms of heat of fusion seems to be slightly higher for the cyclic than for the linear samples (48% as compared to 47%). This trend is in accordance with the crystallinity results obtained after isothermal crystallization.

Literature data determined from nonisothermal DSC measurements of high molecular weight polymer rings are ambiguous. For example, from investigation of PE macrocycles Bielawski et al.[40] find an increase of crystallization and melting temperature of the ring chains by about 2 °C in comparison to the linear analogues (for heating rates of 10 K/min). However, Lecomte et al.[39] report on measurements of cyclic PεCL ($M_{n,lin}$ = 24.0 kg/mol, heating rate 10 K/min) showing a significant reduction of crystallization and melting temperature (~5 to 7 °C) and crystallinity (~27.5%) of the cyclic chains as compared to linear ones of the same chain length.

Here, we intend to state the difficulty of interpreting such nonisothermally detected data, being simultaneously influenced by effects of nucleation and crystal growth and depending drastically on the chosen temperature program. By using nucleating agents, we can separate the information about crystal growth (we are interested in) from nucleation effects, as all samples are nucleated to the same amount.

For this reason we blended the pair of linear and cyclic PεCL samples mentioned above ($M_{n,lin}$ = 35.9 kg/mol) with 1.5 wt % of 1,3:2,4-di(4-chlorobenzylidene)sorbitol (DBS) as a nucleating agent following procedures described by Wangsoub et al.[79] For the nucleated samples we find an accelerated (isothermal) crystallization (f_c was tracked by ^{1}H NMR as described in the previous subsection). Furthermore, the melt memory effect (i.e., the increase of the crystallization temperature after melting the material at rather low temperature T_s), present in the non-nucleated samples up to $T_s \sim$ 86 °C, dissapears for nucleated

samples. Yet, the crystallization temperature from nonisothermal crystallization is increased by ~6 to 9 °C . In contrast to the results for the non-nucleated samples the differences in crystallization temperature T_c and crystallinity f_c between linear and cyclic samples are significantly enlarged for the nucleated ones. T_c and f_c of the cyclics are higher by ~2 °C and 5%, respectively, than for the corresponding linear sample (T_c ~ 45.6 °C as compared to 43.7 °C and f_c ~51% as compared to 46%). For illustration, Figure 12 shows a comparison of heat flow curves from the (second) cooling scan for linear and cyclic PεCL with and without nucleating agent.

Our results confirm that the method of externally controlled heterogeneous nucleation works well to extract information about crystal growth from nonisothermal crystallization data. Since we have ensured that nucleation kinetics is equal for both the linear and the cyclic sample, differences in crystallization temperature can only be related to lamella growth kinetics. The earlier onset of crystallization for the cyclics (the higher T_c value) therefeore strongly implies faster lamellar growth than compared to the linear analogues, yielding a higher crystallinity as an outcome.

CONCLUSIONS

Linear and cyclic poly(ε-caprolactones) (PεCL) were synthesized in a molecular-weight range of 15 kg/mol to 110 kg/mol by tin-based insertion polymerization reactions and characterized by GPC, melt rheology and ^{1}H low-field solid-state NMR and DSC experiments. Detailed investigations have been performed for $M_{n,lin}$ between 50 and 80 kg/mol. The stability of the rings was assessed in a cleavage experiment of a linear polymer PεCL$_n$-O-SnR$_2$-O-PεCL$_m$, for which the separation into PεCL$_n$ and PεCL$_m$ is easily monitored by GPC. We found that degradation of bulk PεCL at 95 °C for some hours is virtually absent when moisture and oxygen are excluded, which means that further contamination in the course of our experiments can be neglected.

The rheological data revealed about a factor of 2 lower viscosities of the cyclic samples as compared to their linear counterparts, which proves the successful synthesis of ring structures. Yet some contamination with opened linear structures cannot be excluded.

The NMR T_2 data show that the T_2 relaxation time of molten rings is significantly longer than that of equivalent linear chains, indicating less (or no) entanglement or packing effects and/or less time needed by the cyclic chains to perform isotropic large-scale chain dynamics. Results from MQ NMR measurements confirm that compared to the linear chains, a lower residual order of chain segments is present in rings due to less or weaker topological restrictions to chain motion. From the MQ data it is evident that at the temperature of the measurement the loss of orientational memory is faster for the cyclics when compared to their linear analogues. The NMR results on chain mobility reflect data from literature, revealing higher overall mobility of cyclics in the melt, compared to their linear counterparts.

Summing up the trends from isothermal crystallization (NMR and DSC) experiments, significant differences between cyclic and linear PεCLs were observed. For cyclic PεCL isothermal crystallization leads to larger crystallinities than for the linear polymers. Results obtained from DSC and NMR after isothermal crystallization match well, confirming the applicability of NMR MSE measurements for the determination of polymer crystallinity. To obtain information on crystallization also from standard DSC methods investigating nonisothermal crystallization, we performed measurements on nucleated PεCL samples giving us the chance to separately explore the effect of crystal growth. This way we could reproduce trends achieved for non-nucleated samples but with significantly enhanced effects. Here, the crystallization was faster for the cyclic counterpart (as the nonisothermal onset T_c was higher than that for the corresponding linear sample), yielding a higher crystallinity. Note that we do not expect large effects of missing chain ends in the cyclics on the fold surface energy of the crystals and on the crystallization process as for the high molecular weights used the chain end concentration in the fold surface (roughly estimated for an adjacent reentry scenario and a realistic lamella thickness of 7.5 nm) does not exceed 5%.

The findings could be interpreted as follows. Given that rings exhibit larger crystallinities when crystallized isothermally *and* nonisothermally, we suggest that the enhanced mobility of the rings (which is reflected in the T_2 and MQ NMR data as well as the rheology results) allows for the formation of a more perfect morphology and thus higher crystallinity. Preliminary spin diffusion NMR experiments indicate that this is accompanied by the formation of thicker crystalline lamellae. Ongoing work is dedicated to the elaboration of trends for the domain sizes.

ASSOCIATED CONTENT

ⓈSupporting Information. Details on the characterization of the samples by solution-state NMR and MALDI−TOF mass spectrometry. This material is available free of charge via the Internet at http://pubs.acs.org.

AUTHOR INFORMATION

Corresponding Author
*E-mail: (K.Sch.) kerstin.schaeler@physik.uni-halle.de; (K.Sa.) kay.saalwaechter@physik.uni-halle.de.

ACKNOWLEDGMENT

REFERENCES

(1) Lauritzen, J. I.; Hoffman, J. D. *J. Res. Natl. Bur. Stand., Sect. A: Phys. Chem.* **1960**, *64*, 73–102.

(2) Strobl, G. *Eur. Phys. J. E* **2000**, *3*, 165–183.

(3) Muthukumar, M. *Lect. Notes Phys.* **2007**, *714*, 1–18.

(4) Olmsted, P. D.; Poon, W. C. K.; McLeish, T. C. B.; Terrill, N. J.; Ryan, A. J. *Phys. Rev. Lett.* **1998**, *81*, 373–376.

(5) Bu, H. S.; Gu, F. M.; Bao, L. R.; Chen, M. *Macromolecules* **1998**, *31*, 7108–7110.

(6) Psarski, M.; Piorkowska, E.; Galeski, A. *Macromolecules* **2000**, *33*, 916–932.

(7) Umemoto, S.; Okui, N. *Polymer* **2002**, *43*, 1423–1427.

(8) Hu, W.; Frenkel, D.; Mathot, V. B. F. *Macromolecules* **2003**, *36*, 8178–8183.

(9) Xiao, Z. G.; Sun, Q.; Xue, G.; Yuan, Z. R.; Dai, Q. P.; Hu, Y. L. *Eur. Polym. J.* **2003**, *39*, 927–931.

(10) Mandelkern, L. *Crystallization of Polymers: Kinetics and Mechanisms*, 2nd ed.; Cambridge University Press: Cambridge, U.K., 2004; Vol. 2.

(11) Hikosaka, M.; Watanabe, K.; Okada, K.; Yamazaki, S. *Interphases and mesophases in polymer crystallization III*; Advances in Polymer Science 191; Springer-Verlag: Berlin, 2005; pp 137−186.

(12) Lippits, D. R.; Rastogi, S.; Hohne, G. W. H.; Mezari, B.; Magusin, P. C. M. M. *Macromolecules* **2007**, *40*, 1004–1010.

(13) Yu, X.; Kong, B.; Yang, X. *Macromolecules* **2008**, *41*, 6733–6740.

(14) Doye, J. P. K.; Frenkel, D. *Phys. Rev. Lett.* **1998**, *81*, 2160–2163.

(15) Hoffman, J.; Miller, R. *Polymer* **1997**, *38*, 3151–3212.

(16) Xu, L.; Fan, Z. Y.; Zhang, H. D.; Bu, H. S. *J. Chem. Phys.* **2002**, *117*, 6331–6335.

(17) Iwata, K. *Polymer* **2002**, *43*, 6609–6626.

(18) Strobl, G. *Prog. Polym. Sci.* **2006**, *31*, 398–442.

(19) Obukhov, S. P.; Rubinstein, M.; Duke, T. *Phys. Rev. Lett.* **1994**, *73*, 1263–1266.

(20) Kapnistos, M.; Lang, M.; Vlassopoulos, D.; Pyckhout-Hintzen, W.; Richter, D.; Cho, D.; Chang, T.; Rubinstein, M. *Nat. Mater.* **2008**, *7*, 997–1002.

(21) McLeish, T. *Science* **2002**, *297*, 2005–2006.

(22) Roovers, J. *Macromolecules* **1988**, *21*, 1517–1521.

(23) McKenna, G. B.; Hostetter, B. J.; Hadjichristidis, N.; Fetters, L. J.; Plazek, D. J. *Macromolecules* **1989**, *22*, 1834–1852.

(24) Cosgrove, T.; Griffiths, P. C.; Hollingshurst, J.; Richards, R. D. C.; Semlyen, J. A. *Macromolecules* **1992**, *25*, 6761–6764.

(25) Habuchi, S.; Satoh, N.; Yamamoto, T.; Tezuka, Y.; Vacha, M. *Angew. Chem., Int. Ed.* **2010**, *49*, 1418–1421.

(26) Ungar, G.; Zeng, K. B. *Chem. Rev.* **2001**, *101*, 4157–4188.

(27) Cooke, J.; Viras, K.; Yu, G. E.; Sun, T.; Yonemitsu, T.; Ryan, A. J.; Price, C.; Booth, C. *Macromolecules* **1998**, *31*, 3030–3039.

(28) Dodgson, K.; Semlyen, J. A. *Polymer* **1977**, *18*, 1265–1268.

(29) Higgins, J. S.; Dodgson, K.; Semlyen, J. A. *Polymer* **1979**, *20*, 553–558.

(30) Dodgson, K.; Bannister, D. J.; Semlyen, J. A. *Polymer* **1980**, *21*, 663–667.

(31) Semlyen, J. A. *Pure Appl. Chem.* **1981**, *53*, 1797–1804.

(32) Higgins, J. S.; Ma, K.; Nicholson, L. K.; Hayter, J. B.; Dodgson, K.; Semlyen, J. A. *Polymer* **1983**, *24*, 793–799.

(33) Clarson, S. J.; Dodgson, K.; Semlyen, J. A. *Polymer* **1985**, *26*, 930–934.

(34) Orrah, D. J.; Semlyen, J. A.; Rossmurphy, S. B. *Polymer* **1988**, *29*, 1452–1454.

(35) Cosgrove, T.; Turner, M. J.; Griffiths, P. C.; Hollingshurst, J.; Shenton, M. J.; Semlyen, J. A. *Polymer* **1996**, *37*, 1535–1540.

(36) Laurent, B. A.; Grayson, S. M. *Chem. Soc. Rev.* **2009**, *38*, 2202–2213.

(37) Kricheldorf, H. R. *J. Polym. Sci., Part A: Polym. Chem.* **2010**, *48*, 251–284.

(38) Narumi, A.; Zeidler, S.; Barqawi, H.; Enders, C.; Binder, W. H. *J. Polym. Sci., A: Polym. Chem.* **2010**, *48*, 3402–3416.

(39) Li, H.; Jérôme, R.; Lecomte, P. *Polymer* **2006**, *47*, 8406–8413.

(40) Bielawski, C. W.; Benitez, D.; Grubbs, R. H. *Science* **2002**, *297*, 2041–2044.

(41) Cho, T.-Y.; Stille, W.; Strobl, G. *Colloid Polym. Sci.* **2007**, *285*, 931–934.

(42) Hertlein, C.; Saalwächter, K.; Strobl, G. *Polymer* **2006**, *47*, 7216–7221.

(43) Kohn, P.; Strobl, G. *Macromolecules* **2004**, *37*, 6823–6826.

(44) Men, Y. F.; Rieger, J.; Strobl, G. *Phys. Rev. Lett.* **2003**, *91*.

(45) Heck, B.; Sadiku, E. R.; Strobl, G. R. *Macromol. Symp.* **2001**, *165*, 99–113.

(46) Bittiger, H.; Marchessault, R. H.; Niegisch, W. D. *Acta Crystallogr., Sect. B: Struct. Crystallogr. Cryst. Chem.* **1970**, *B 26*, 1923–1927.

(47) Kaji, H.; Horii, F. *Macromolecules* **1997**, *30*, 5791–5798.

(48) Hu, W.-G.; Schmidt-Rohr, K. *Acta Polym.* **1999**, *50*, 271–285.

(49) Hoskins, J. N.; Grayson, S. M. *Macromolecules* **2009**, *42*, 6406–6413.

(50) Choi, J.; Chun, S.-W.; Kwak, S.-Y. *J. Polym. Sci., Part B: Polym. Phys.* **2007**, *45*, 577–589.

(51) Nunez, E.; Vancso, G. J.; Gedde, U. W. *J. Macromol. Sci., Part B: Phys.* **2008**, *47*, 589–607.

(52) Saalwächter, K. *Prog. Nucl. Magn. Reson. Spectrosc.* **2007**, *51*, 1–35.

(53) Maus, A.; Hertlein, C.; Saalwächter, K. *Macromol. Chem. Phys.* **2006**, *207*, 150–1158.

(54) Clauss, J.; Schmidt-Rohr, K.; Spiess, H. W. *Acta Polym.* **1993**, *44*, 1–17.

(55) Mauri, M.; Thomann, Y.; Schneider, H.; Saalwächter, K. *Solid State Nucl. Magn. Reson.* **2008**, *34*, 125–141.

(56) Kricheldorf, H. R.; Eggerstedt, S. *Macromolecules* **1998**, *31*, 6403–6408.

(57) Kricheldorf, H. R.; Lee, S. R. *Macromolecules* **1995**, *28*, 6718–6725.

(58) McKenna, G. B.; Hadziioannou, G.; Lutz, P.; Hild, G.; Strazielle, C.; Straupe, C.; Rempp, P.; Kovasc, A. J. *Macromolecules* **1987**, *20*, 498–512.

(59) Hahn, E. L. *Phys. Rev.* **1950**, *80*, 580–594.

(60) Saalwächter, K. *Macromolecules* **2005**, *38*, 1508–1512.

(61) Vaca Chávez, F.; Saalwächter, K. *Macromolecules* **2011**, *44*, 1549–1559.

(62) Vaca Chávez, F.; Saalwächter, K. *Phys. Rev. Lett.* **2010**, *104*, 198305.

(63) Vaca Chávez, F.; Saalwächter, K. *Macromolecules* **2011**, *44*, 1560–1569.

(64) Herrmann, A.; Novikov, V. N.; Rössler, E. A. *Macromolecules* **2009**, *42*, 2063–2068.

(65) Acierno, S.; Di Maio, E.; Iannace, S.; Grizzuti, N. *Rheol. Acta* **2006**, *45*, 387–392.

(66) Gimenez, J.; Cassagnau, P.; Michel, A. *J. Rheol.* **2000**, *44*, 527–547.

(67) Grimau, M.; Laredo, E.; Perez, M. C. Y.; Bello, A. *J. Chem. Phys.* **2001**, *114*, 6417–6425.

(68) Herrera, D.; Zamora, J. C.; Bello, A.; Grimau, M.; Laredo, E.; Müller, A. J.; Lodge, T. P. *Macromolecules* **2005**, *38*, 5109–5117.

(69) Charlesby, A.; Bridges, B. J. *Radiat. Phys. Chem.* **1982**, *19*, 155–165.

(70) Hansen, E. W.; Kristiansen, P. E.; Pedersen, B. *J. Phys. Chem. B* **1998**, *102*, 5444–5450.

(71) Derbyshire, W.; van den Bosch, M.; van Dusschoten, D.; MacNaughtan, W.; Farhat, I. A.; Hemminga, M. A.; Mitchell, J. R. *J. Magn. Reson.* **2004**, *168*, 278–283.

(72) Abragam, A. *The principles of nuclear magnetism*; Clarendon Press: Oxford, 1961.

(73) Demco, D. E.; Johansson, A.; Tegenfeldt, J. *Solid State Nucl. Magn. Reson.* **1995**, *4*, 13–38.

(74) Crescenzi, V.; Manzini, G.; Calzolar, G.; Borri, C. *Eur. Polym. J.* **1972**, *8*, 449–463.

(75) Khambatta, F. B.; Warner, F.; Russell, T.; Stein, R. S. *J. Polym. Sci., Part B: Polym. Phys.* **1976**, *14*, 1391–1424.

(76) Pyda, M. ATHAS Data Bank. 2010; http://athas.prz.edu.pl/.

(77) Schick, C. *Anal. Bioanal. Chem.* **2009**, *395*, 1589–1611.

(78) Wurm, A.; Merzlyakov, M.; Schick, C. *J. Therm. Anal. Calorim.* **1999**, *56*, 1155–1161.

(79) Wangsoub, S.; Davis, F. J.; Mitchell, G. R.; Olley, R. H. *Macromol. Rapid Commun.* **2008**, *29*, 1861–1865.